ChemComm

Synthesizing and Formulating Metal Oxide Nanoparticle Inks for Perovskite Solar Cells.

Journal:	*ChemComm*
Manuscript ID	CC-FEA-06-2023-002830.R2
Article Type:	Feature Article

ARTICLE

Synthesizing and Formulating Metal Oxide Nanoparticle Inks for Perovskite Solar Cells

Received 00th January 20xx,
Accepted 00th January 20xx

DOI: 10.1039/x0xx00000x

Peter Armstrong,[a] Sashil Chapagain,[a] Rojita Panta,[a] Craig Grapperhaus,[a] and Thad Druffel [b*]

The perovskite solar cell has commercial potential due to the low-cost of materials and manufacturing processes with cell efficiencies on par with traditional technologies. Nanomaterials have many properties that make them attractive for the perovskite devices, including low-cost inks, low temperature processing, stable material properties and good charge transport. In this feature article, the use of nanomaterials in the hole transport and electron transport layers are reviewed. Specifically, SnO_2 and NiO_x are the leading materials with the most promise for translation to large scale applications. The review includes a discussion of the synthesis, formulation, and processing of these nanoparticles and provides insights for their further deployment towards commercially viable perovskite solar cells.

1.0 Introduction

The perovskite solar cell (PSC) has generated a fair amount of interest due to the low cost of materials and manufacturing with a reported highest efficiency of 26.1%, which is on par with traditional technologies of silicon (26.8%) and CdTe (22.3%).[1] The structure of the PSC includes a perovskite (PVSK) thin film that is sandwiched between two charge extraction layers, the electron transport layer (ETL) and hole transport layer (HTL). The technology also lends itself well to tandem devices including PVSK/silicon (33.7%), PVSK/CIGS (24.2%) as well as PVSK multifunction devices (26.4%).[2] All of these devices utilize hole transport or electron transport layers that are carbon based. Nanoparticles can play a very important role in the commercialization of the PSC, since these can be made from earth abundant materials, easy to scale, have suitable band alignment and can impart improved durability.

A technoeconomic analysis demonstrated how using nanoparticles for the charge transport layers in a perovskite film can achieve a cost of $0.04-$0.10 per watt. Key to this low cost is large area rapid coating on a roll-to-roll system and reduced energy consumption by utilizing IPL annealing. Several recent reviews have examined current efforts in large area perovskite coatings with focus on device architecture and performance.[3-6] However, the discussion on the formulation of charge transport material inks, has largely been centered on polymer materials. This focus on polymers has ignored the versatility, innate stability, and scalable nature of metal oxide nanoparticles. Made from earth abundant materials and easily customized to meet specific applications requirements metal oxides are well positioned to make the transition from laboratory to production line applications in solar. Therefore, a review of some of the leading inorganic nanoparticles is warranted with a focus on synthesis, ink formulation and the resulting performance towards a scalable manufacture of perovskite films (Figure 1).

Worth a special note, metal oxide nanoparticles have also been used to dope the perovskite lattice forming bulk heterojunction PSC's. The nanoparticles initiate heterogeneous nucleation during film formation which accelerates crystal growth resulting in larger grain growth and film density.[7 8, 9] Nanoparticle doping of the perovskite also increases the p-type character or the n-type character of the perovskite depending on the dopant added. This doping increases the charge carrier concentration in the perovskite and accelerating charge extraction.[10] Heterojunction devices have also shown promising increased in stability when compared with undoped films.[11]

The specific nanoparticle materials for the HTL and ETL are typically metal oxides that can be very straightforward to synthesize and disperse in solvents suitable for volume manufacturing. The functionalization schemes of these metal oxides have been studied at length to improve dispersion in selected solvents and to establish homogeneous inorganic/organic thin films. This solvent engineering scheme has resulted in the capability to deposit a SnO_2 ink directly onto a PVSK thin film yielding an efficiency of 16.5% using a flexible polymer substrate.[12] Similarly, aqueous based SnO_2 dispersions have in the past few years been the workhorse of low temperature PSC manufacturing with over 500 papers and efficiencies on glass of 23.32%[13] and plastic of 20.1%[14].

A general synthesis path for metal oxides is to take a solution of the target metal salt and react it with a base to precipitate the oxide or hydroxide of that metal. This reaction can be controlled by the addition of ligands or surfactants during synthesis to control particle size and solubility. After synthesis the nanoparticles can be formulated into inks through the addition of additives, solvent engineering, or further particle

[a] University of Louisville, Department of Chemistry, Louisville, KY 40292.
[b] University of Louisville, Conn Center for Renewable Energy Research, Louisville, KY 40292.
* Thad.druffel@louisville.edu
†

functionalization. Together the properties selected for during synthesis and ink formulation drive the materials performance. By evaluating the approaches taken during the synthesis and ink formulation in the context of final device performance future work can build off previous success.

The primary role of an ETL in PSCs is to enable efficient extraction of photogenerated electrons from the PVSK absorber layer and transport them to the electrode, while concurrently inhibiting hole transport, thus reducing charge recombination probability. Moreover, the ETL acts as a protective barrier between the PVSK and the electrode, mitigating the degradation of the PVSK layer due to contact with the metal electrode. Various binary and ternary metal oxides, including TiO_2, ZnO, SnO_2, WO_3, In_2O_3, Nb_2O_5, Fe_2O_3, Cr_2O_3, CeO, $BaSnO_3$, $SrSnO_3$, $BaTiO_3$, $SrTiO_3$, Zn_2SO_4, Nb_2O_5, and $BaSnO_3$, have been explored as ETLs in n–i–p configurations.[15-17] Of these TiO_2, ZnO and SnO_2 have been demonstrated as effective inorganic ETLs. Organic nanomaterials, such as C60, C70, PC61BM, and PC71BM, as well as a variety of fullerene derivatives and their corresponding different isomeric functionalized fullerene structures, have been investigated in p–i–n configurations, where the ETL is deposited directly on the PVSK thin film. For this review, we will focus on SnO_2 as recent developments has demonstrated it to be effective in both n-i-p and p-i-n configurations with little to no annealing necessary when deposited from solution phase.

HTL materials face many of the same considerations as ETLs for material characteristics but with the electronics targeting hole transport instead of electron transport. Favored for their stability over organic alternatives and good band alignment with the valence band of the PVSKs; NiO_x, Cu_xO, CuI, CuSCN, and CuS, have been explored as HTLs through a variety of methods. Inorganic copper salts such as CuSCN, CuI, and CuS have shown promise as inorganic options for devices of n-i-p configuration.[18] However, they struggle with conductivity and reactivity with deposited metal contacts. Copper oxide nanoparticles are also an active field of work with delafossite like composition ($CuM^{3+}O_2$) recently emerging as a promising solution to the instability of Cu_2O.[19] To date, copper oxide nanoparticles trail nickel oxide (NiO_x) in terms of conductivity and device performance, which has been the most successful inorganic HTL to date. Due to its natural self-doping p-type character NiO_x has shown high hole carrier densities, conductivity, and good band alignment with PVSKs. These properties make it a natural choice for use as an HTL.

Under ambient conditions PVSK solar cells undergo degradation resulting in structural and morphological changes that decrease cell performance. Because of this instability, commercialization of PVSKs face a significant challenge.[20] Nanomaterials, and nanomaterial polymer composites are actively being studied for PVSK encapsulation. These nanomaterials create a protective barrier from moisture, oxygen, and temperature thus improving cell performance and stability. Carbonaceous materials like graphene and its derivatives have unique properties such as mechanical flexibility, solution processability, hydrophobicity, and high thermal stability. Further functionally can be added by utilizing graphene's versatile surface chemistry. In sum the properties of graphene make it a prime candidate for use as an encapsulation material.[21]

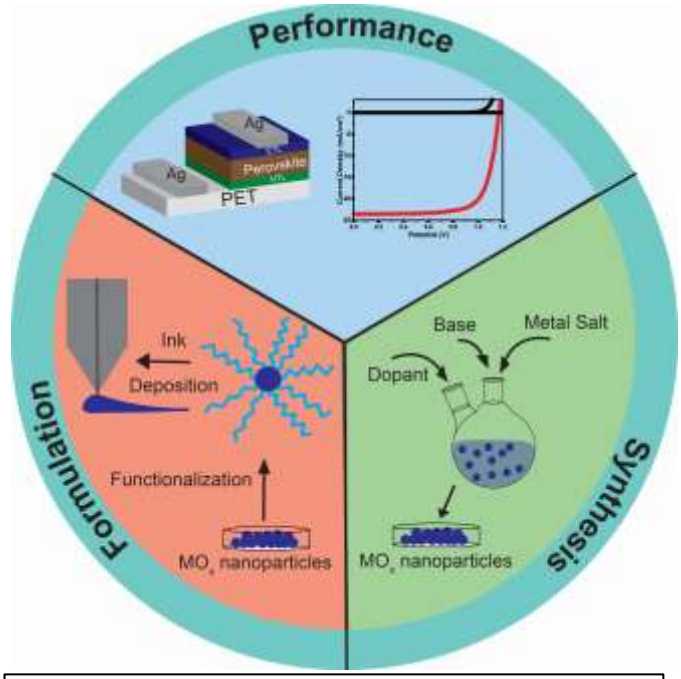

Figure 1. Scheme of the cyclic relationship between particle synthesis, ink formulation, and device performance. Each step influencing the next one and providing feedback to the previous steps

This feature article reviews the literature surrounding the production of SnO_2 and NiO_x metal oxide nanoparticles for ETL and HTL layers as well as utilization of carbon nanomaterials as encapsulation layers. SnO_2 and NiO_x are the leading CTL materials with the most promise for translation from laboratory scale to industrial scale applications. This review provides a summary of the current state of research for these materials with an emphasis on the synthesis and formulation instead of performance. How synthesis and ink formulation play into performance can provide insights for future work. As such each of the synthesis, formulation, deposition, post processing, and annealing applications are discussed, with a perspective towards scaling to terawatt production instead of champion performance. Finally, an outlook for the utilization of nanoparticles for PSC is offered. Ultimately the cost of the materials and device manufacturing as well as the efficiency and reliability will drive the adoption of nanoparticles within the PSC.

2.0 Nanomaterials for Devices

2.1 Electron Transport Layer

For an ETL material to be effective it needs to have a conduction band that is slightly lower than that of the PVSK, while also having a deep valence band to prevent electron-hole recombination. This wide band gap is also important for insuring high transparency and maximum light adsorption by the PVSK layer. Additionally, the selected material needs to have high electron mobility to reduce internal series resistance and increase charge extraction. A uniform and pinhole-free ETL is

essential to prevent direct contact between the PVSK and HTLs, which could lead to charge recombination and device degradation. As PVSK research moves to improving stability and scalability the extra considerations of environmentally stable and process compatibility are now also being considered.

Developed initially in dye-sensitized solar cells, TiO_2 was the first ETL material used in a PVSK sensitized solar cell during the pioneering work of Miyasaka's team in 2009.[22] Since then, the application and optimization of TiO_2 have progressively evolved, and improved with it playing a major role in the development of mesoporous PVSK architectures. TiO_2 has been the dominate ETL material used for mesoporous architectures that are effective but complex requiring time-consuming methods and high-temperature sintering. This renders mesoporous structures unsuitable for scaling up PVSK solar cells for commercial use.

Transitioning from the complex mesoporous scaffold to a simpler planer structure was demonstrated as feasible by Snaith et al. in 2013. Their initial report on planar PSCs employed TiO_2 as a compact layer and achieved a power conversion efficiency (PCE) of 4.9%.[23] Snaith et al. followed this initial result with a vapor phase deposited PVSK on compact TiO_2 resulting in a PCE of over 15% accompanied by an open circuit voltage of 1.07 V.[24] This research signified a paradigm shift in PVSK solar cell research, with a simplified planar structure being sufficient to achieve highly efficient PVSK solar cells.

Following this innovation, researchers began to investigate other low-temperature processable ETLs such as ZnO, PCBM, and SnO_2 as potential alternatives to TiO_2 for use in simple planar structures. Currently, tin(IV) oxide (SnO_2) has emerged as a prominent ETL alternative to titanium dioxide (TiO_2) and zinc oxide (ZnO) in PSCs, with the highest reported PCE of 25.7% in single-junction planar structures.[25] SnO_2 is a wide bandgap n-type semiconductor (3.5-4.0eV) that aligns with the conduction band of the PVSKs and is transparent to most visible and UV light. It also has been reported to have high electron mobility (200 to 250 $cm^2/V•S$) while being able to be processed at low temperatures.[26]

SnO_2 exhibits superior photostability compared to TiO_2, particularly towards ultraviolet (UV) light. This increased photostability addresses the issue of light-induced degradation, a significant problem reported for TiO_2 based PSCs.[27] Chemically, SnO_2 exhibits good stability in the presence of moisture and oxygen and its hygroscopic nature is less pronounced compared to TiO_2 and ZnO, making it less prone to degradation in ambient environments.[28] When compared to fullerene derivatives, SnO_2, displays superior thermal and chemical stability. This enhanced stability can potentially lead to improved long-term performance and reduced degradation of PSCs.

The processing temperature requirements for SnO_2 are also lower than those for TiO_2, broadening the range of viable substrates for PSCs fabrication, to include flexible and temperature-sensitive polyethylene terephthalate (PET) based substrates. SnO_2 as an ETL is amenable to a wide variety of deposition methods, such as spin-coating, spray coating, blade coating, and slot die coating. This adaptability introduces greater flexibility into the fabrication process, but most work with SnO_2 uses the n-i-p configuration as the deposition of SnO_2 on top of a PVSK is challenging. Finally, SnO_2 is non-toxic and environmentally friendly, characteristics that enhance its suitability as an ETL material for large-scale production and application of PSCs.

It is worth mentioning some of the work done with fullerene derivatives (C60 and PCBM), since these are often adapted for p-i-n architectures. These fullerene derivatives are favoured due to their facilitation of low-temperature processing via solution or physical vapor deposition, superior electron mobility, and tuneable LUMO energy levels, which match well with the energy band of PVSK. [29] They are also often employed in bilayer structures with additional metal oxide ETLs (fullerene/MO_x ETL), a common approach taken to enhance the performance of PSCs. The improvement in efficiency is primarily attributed to the defect passivation properties of fullerenes, which in turn improves stability.[30, 31] However, a significant impediment to the widespread adoption of these materials in commercial applications is the extremely high production costs associated with fullerenes. As such, the development of cost-effective alternatives to these ETL materials for inverted PVSK solar cells is critical for facilitating broader commercialization of this promising technology.

The low-temperature fabrication methodologies of SnO_2 have provided its suitability for the development of flexible PSCs on low temperature substrates.[32, 33] Standard flexible plastic substrates like PET (Tg: 70–110 °C) and polyethylene naphthalate (PEN) (Tg: 120–155 °C) are capable of withstanding limited heating, but are incompatible with higher temperature precursor or mesoporous annealing conditions. Low temperature work by Song et al. and Qi Jiang et al. have demonstrated up to 21.6% PCE using commercially available SnO_2 nanoparticles. [34-36] As flexible modules and roll to roll processing become more common, colloidal SnO_2 nanoparticles have been deemed a promising route to formulate the ETL for flexible PSCs. The utilization of nanoparticles circumvents the high-temperature sintering process, which would otherwise be integral in the transition from precursors to SnO_2 films. Additionally, pre-synthesized nanoparticles can be suspended in an array of solvents that are compatible with PVSK enabling direct coating on the PVSK layer to serve as an upper charge transport layer (CTL). Consequently, the utilization of pre-synthesized SnO_2 nanoparticles simplifies the process and holds the potential to shorten the total fabrication time.

The synthesis of SnO_2 nanoparticles is generally achieved through precipitation, solvothermal, hot injection, and the inverse micelle-water injection methods.[32, 33, 37, 38] These processes result in the formation of pre-synthesized SnO_2 nanoparticles, which are subsequently deposited onto a substrate to form a film. A distinct advantage of synthesized nanoparticles is the ability to engineer surface ligands and solubility to fit a desired application (Table 1). An example of this is the work of Xie et al. where they developed highly crystalline SnO_2 nanoparticles with superior dispersibility in non-polar solvents utilizing a solvothermal method. Using spin-

coating they were able to deposit a high quality SnO_2 film on ITO-PEN that had a PCE of 13.90%[33] Park et al. engineered ultrafine SnO_2 quantum dots (QD) capped with a liable ligand where the ligands spontaneously exchanged with halides in a PVSK solution as part of the coating process, leading to an appropriate SnO_2 QD–halide junction resulting in a PCE of 17.7% with a short circuit current density (J_{sc}) of 19.7 mA cm^{-2}, open circuit voltage (V_{oc}) of 1.13 V, and a fill factor (FF) of 79.0%. [32]

Along with ligands and solubility, the electrical properties of nanoparticles can be tuned by the introduction of dopants to the crystal lattice. Doping of semiconducting metal oxides (MO_x) effectively modulates electrical properties such as carrier concentration and electron mobility, in addition to altering optical and structural properties. Common doping methodologies can be categorized as equivalent cation doping in which the material is doped with an ion of the same oxidation state, and nonequivalent cation doping in which the material is doped with an ion of higher or lower oxidation state. Equivalent cation doping improves defect densities, improves carrier mobility, and induce alterations in the energy band structure, which can lead to diminished trap-state density and promoted energy band alignment with PVSK. Noh et al. demonstrated Zr doping in SnO_2 that resulted in a conduction band up shift which increased the built in potential and improved the band alignment with the PVSK with a champion device achieving a PCE of 19.54%.[39]

Nonequivalent doping directly effects the electron density of the conduction band. Specifically, the incorporation of lower valence cations such as Li^+,[47] Mg^{2+}, Zn^{2+},[48] Y^{3+}, and Al^{3+} into the crystal lattice of tetravalent Sn^{4+} or Ti^{4+} results in p-type doping, while the incorporation of higher valence cations like Nb^{5+}, [49] and W^{6+} yields n-type doping. The incorporation of higher valence cations, n-type doping, enhances the electron density causing a more positive shift in the conduction band. Together the shifted conduction band and increased electron density increase film conductivity.[40, 50, 51] Ren and associates report a 2.44% increase in PCE using Nb-doped SnO_2. [49] P-type doping decreases the electron density of the conduction band while upshifting the Fermi level and decreasing the oxygen vacancies. This promotes electron transport while impeding charge recombination at the ETL/PVSK interface. [48] Yang et al. reported

Table 1: Survey of recent works using SnO_2 as the ETL. SC: Spin-coating,

Device architecture	ETL	Deposition	Processing	J_{sc}	V_{oc}	FF	PCE	Ref
Regular (P-I-N) architecture								
Sb:SnO_2/ $MAPbI_3$/ spiro-OMeTAD/ Au	NC	SC	100°C, 30 min	22.6	1.06	72.0	17.2	[40]
PEN/ ITO/ $MAPbI_3$/ spiro-OMeTAD/ Au	NC	SC	80°C, 15min	19.7	1.13 V	79.0%	17.7%	[32]
ITO/ SnO_2/ $(FAPbI_3)_x(MAPbBr_3)_{1-x}$/ Spiro-OMeTAD/ Au	NC	SC	150°C, 30 min	24.87	1.09V	74.77%	20.27%	[35]
ITO/ SnO_2/ $(FAPbI_3)_x(MAPbBr_3)_{1-x}$/ Spiro-OMeTAD/ Au	NC	SC	150°C, 30 min	25.2	1.18	78.4%	23.32%	[13]
ITO/ SnO_2/ $MAPbI_3$/ Spiro-OMeTAD/ MoOx/Ag	NC	Slot-die	Air-knife, IPL	23.70	0.91	52.0	11.24	[41]
ITO/ SnO_2/ $MAPbI_3$/ Spiro-OMeTAD/ Au	NC	Blade	100°C	22.86	1.124	76.17%	19.6	[42]
ITO/SnO_2/ $Cs_{0.05}FA_{0.85}MA_{0.15}PbI_{2.9}Br_{0.15}$/ Spiro-OMeTAD/Au	NC	Spray	150°C, 30 min	23.35	1.14	66.6	17.78	[43]
Inverted(N-I-P) architecture								
glass/ ITO/ NiO_x/ $MAPbI_3$/ ZnO/ Al	NC	SC	N/A	21.0	1.01	76	16.1	[44]
Glass- ITO/ PTAA/ PFN/ $MAPbI_3$/ SnO_2-A/Ag.	NC	Blade	100°C, 10 min	22.6	1.02	61.0	14.1	[45]
PET/ ITO/ PTAA/ PFN/ $MAPbI_3$/ Y:SnO_2-A/ BCP/ Ag	NC	Blade	100°C for 2 min	22.38	1.08	68.4%	16.5%	[12]
PET/ ITO/ PTAA/ PFN/ FAMAPbIBr/ Y:SnO_2-A/ BCP/ Ag	NC	Blade	IPL	23.7	1.09	65.7	16.9	[46]

the Y doping led to a more positive conduction band minimum in Y-SnO_2 improving conductivity and charge extraction. [52]

As mentioned before, one of the benefits of nanoparticles is their adaptability to a variety of solution deposition methods. Solution deposition methods are widely employed due to their cost-effectiveness, ease of implementation, and versatility. Various deposition methods, including spin-coating, chemical bath deposition (CBD), spray pyrolysis, screen printing, blade-coating, and slot-die coating, can achieve solution-processed deposition.[53-55] Currently spin-coating is the most common method utilized in lab scale research but interest is increasing in larger area depositions. A recent study by Siegrist et al. on the effect of blade coating parameters including blade speed, blade gap, ink concentration and volume, and stage heating. They conclude that of blade coating of large area devices is best performed using a continuous solution supply with blade coating and further development of slot die coating.[56]

Bu et al. demonstrated an interface passivation strategy with potassium treatments for SnO_2 ETLs to obtain high-efficiency and hysteresis-free low-temperature fabricated PSCs. After the treatment of pre-synthesized SnO_2 with potassium, they were able to achieve a PCE of 20.50% for rigid PSCs and a PCE of 17.18% for flexible PSCs on a small area device of 0.16 cm^2. Additionally, they also obtained a high PCE of 15.22% for flexible PSCs based on slot-die-coated commercial SnO_2 and a PCE of 14.89% with their synthesized SnO_2 NCs. The addition of the K ions in the interface forms KBr that thus passivates the surface defects of the PVSK to promote high performance and hysteresis-free properties. [57]

Dou et al. demonstrated blade coating of a commercial SnO_2 nanoparticle dispersion achieving a PCE up to 19.6% with an V_{oc} of 1.124 V. Using a slot-die coating on glass-ITO/SnO_2, they achieved a PCE of 17.31% and V_{oc} of 1.111 V, and FF of 69.5%.[42]

Taheri et al. developed a simple and scalable deposition approach based on automated spray-coating to prepare uniform and dense SnO_2 ETLs achieving a PCE of 15.3% on a flexible substrate with reduced device hysteresis.[58]

In the space of scalable deposition methods, we have explored the use of ink jet printing and roll to roll slot die coating. Working with a commercially available water based SnO_2 suspension, we demonstrated successful SnO_2 coatings, annealed using intense pulsed light (IPL) annealing. The advantage of IPL annealing lies in its rapid delivery of high energy density over a short interval of time. By applying IPL annealing on ink jet printer SnO_2 we were able to create a uniform film on a glass substrate.[59] On our roll to roll slot die coater, we use a ITO-PET substrate and are able to test large area coatings. We found that the due to the decreased thermal mass of PET as compared to glass, a lower pulse intensity pattern was required for effective annealing without warping of the PET. Additionally the addition of a surfactant was necessary to achieve appropriate wetting on the ITO surface. Using optimized parameters for slot die coated SnO_2 and perovskite we achieved an average PCE of 10.6%, V_{oc} of 0.97 V, J_{sc} of 22.9 mA/cm^2 and FF of 47% for 1 cm^2 cells taken from across a 1 meter length of film.[41]

SnO_2, processed through a solution-based method, has been extensively validated as an ETL material in conventional (n–i–p) structures, with thin films of SnO_2 ETL being directly deposited onto the conductive substrate. However, the direct deposition of solution-processed SnO_2 as an ETL on the top of the PVSK in the p-i-n structure remains relatively unexplored. The lack of direct deposition of solution-processed SnO_2 ETLs in p–i–n structures can be ascribed to the solvent incompatibility with the PVSK absorber layer.[44, 60, 61] The selection of PVSK-compatible solvents is limited, excluding highly polar solvents that are typically requisites for preparing SnO_2 dispersions. Additionally, the conversion of the precursor to SnO_2 on the PVSK surface necessitates prolonged high-temperature annealing, which could potentially instigate the degradation of the underlying PVSK layer.

In most instances, MOx is deposited onto an organic ETL, resulting in bilayers such as PCBM/ZnO, C60/SnO2, and PCBM/SnO2. You et al. reported the development of solution-processed highly stable inverted PSCs, employing p-type NiOx and n-type ZnO nanoparticles as hole and electron transport layers, respectively. The inverted PSCs, configured as glass/ITO/NiO_x/PVSK/ZnO/Al, demonstrated a notable PCE of 16.1%, retaining 90% of the original PCE following 60 days of storage in ambient air at room temperature. [44]

The stability of pre-synthesized MO_x nanoparticle dispersions in desirable solvents can be achieved via the coordination of ligands with MO_x nanoparticles. However, the presence of bulky organic ligands introduces an electrical barrier within the film, mitigating the charge transfer capability of the CTL, and thereby diminishing the overall efficiency of the PSC. To address these challenges, we developed a simple strategy to facilitate the direct deposition of SnO_2 on the PVSK (Figure 2).

We synthesized SnO_2 nanoparticles via a sol-gel technique and subsequently functionalized with acetic acid, yielding acetate-functionalized tin oxide nanoparticles (SnO_2-A). This functionalization permitted the formation of a stable colloidal dispersion of SnO_2-A in anhydrous ethanol. The resultant SnO_2-A dispersion was directly deposited onto a PVSK film. The photovoltaic performance of devices fabricated using this approach attained a maximum PCE of 14.1%.[45] Device efficiency was impeded by a relatively high series resistance, a consequence of insufficient crystallinity associated with the lower-temperature annealing employed for the solution-processed SnO_2 nanoparticles in contrast to the high-temperature annealed SnO_2. To enhance the performance of the low-temperature synthesized SnO_2, yttrium was incorporated into the SnO_2 crystal lattice at an optimized concentration of 2 mol%. After the yttrium doping, the performance of the low-temperature processed flexible PSCs on PET-ITO substrates increased from 14.3% to 16.5% (Figure 3a).[12]

The extended annealing time required by different layers constitutes a significant limiting factor for the rapid, scalable production of PSCs on flexible substrates utilizing high-throughput printing techniques such as the roll-to-roll method. To address this area, we implemented IPL for rapid annealing of the PVSK absorber layer. Utilizing rapid IPL annealing of the PVSK active layer and top coated Y:SnO_2-A we achieved a PCE of

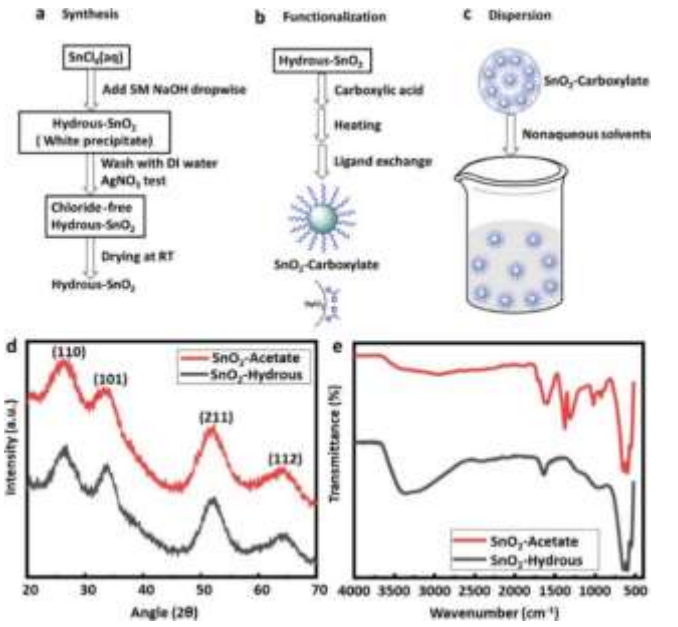

Figure 2. (a–c) Schematic illustration of the synthesis of hydrous-SnO_2, functionalization of hydrous-SnO_2 with acetic acid to yield SnO_2-A, and preparation of a stable colloidal dispersion in anhydrous ethanol and (d,e) XRD patterns and FTIR spectra of hydrous-SnO_2 and SnO_2-A. Reprinted with permission from S. Chapagain, P. S. Chandrasekhar, D. McGott, R. C. Bramante, M. F. van Hest, M. O. Reese, T. Druffel and C. A. Grapperhaus, *ACS Applied Energy Materials*, 2021, **4**, 10477-10483. Copyright 2021 American Chemical Society.

16.7% for blade-coated, flexible, mixed-cation PSCs on ITO-PET substrates in a p-i-n structure (Figure 3b).[46] Annealing of the SnO_2 was facilitated by the PVSK absorbing the photonic energy of the IPL and super heating at the surface.

Overall, pre-synthesized SnO_2 nanoparticle dispersions are emerging as an ideal material for the ETL in PSCs. The employment of nanoparticles circumvents the need for a high-temperature sintering process, typically obligatory in the conversion from precursor to SnO_2 nanoparticles. The low-temperature fabrication methodologies associated with SnO_2 emphasize its suitability for the development of flexible PSCs on substrates comprised of low-melting PET. Nevertheless, the use of SnO_2 nanoparticles as an ETL in PSCs has predominantly been as a base layer directly on the substrate. Our work has shown promise for the direct deposition of SnO_2 onto the PVSK layer and further development in this area is ongoing.

The main challenges in the adoption of SnO_2 as an ETL in p-i-n devices are solvent incompatibility with the perovskite layer and annealing conditions. Solvent incompatibility can be addressed through ligand design as demonstrated with SnO_2-A. Annealing is a major issue as SnO_2 nanoparticles that are either left unannealed or annealed at low temperatures tend to suffer from poor conductivity and overall diminished performance. Thus, future research endeavours should prioritize the enhancement of these nanoparticles' performance. One possible avenue for such improvement could involve modifying the electronic properties through elemental doping or by annealing low temperature processed SnO_2 ETL. The traditional method of hotplate annealing proves ineffective for annealing SnO_2 on the perovskite layer due to the degradation of perovskite at high temperatures. Thus, it becomes necessary to explore alternate annealing techniques apart from hotplate annealing, such as the Intense Pulsed Light (IPL) method.

Annealing of the SnO_2 layer is also critical for device durability as incomplete annealing can exhibit porous characteristics, potentially falling short of providing an adequate barrier to prevent interaction between the top metal contact and perovskite. Hence, further studies are needed to understand the possible interaction at the perovskite/SnO_2/silver interface. The potential interaction can be circumvented by engineering an appropriate interface between either the perovskite and SnO_2, or the SnO_2 and Ag. Lastly, a critical area of study is the long-term stability of PSCs when using SnO_2 as the top layer. This investigation is vital to ensure the extended functionality and viability of these solar cells.

2.2 Hole Transport Layer

Materials for the HTL can include organic compounds, such as 2,2′,7,7′-tetrakis(N,N-di-p-methoxyphenylamine)-9,9′-spirobifluorene (spiro-OMeTAD), poly(3,4-ethylenedioxythiophene) polystyrene sulfonate (PEDOT-PSS), polytriarylamine (PTAA), and polythiophene (PT), and inorganic metal oxides.[62-65] Of the latter, NiO_x is an attractive candidate as it has a tunable valence band sitting at 5.2 eV and a band gap of 3.5 eV that is well aligned for proper p-type conduction with the PVSK valence band of ~5.4 eV for $MAPbI_3$.[65] As such, NiO_x nanoparticle suspensions are widely used in PVSK research; often as independent HTLs or in conjunction with organic polymers.[66] Coated primarily by spin-coating, many devices exceeding 20% on both glass and flexible substrates have been produced using NiO_x.[66-72]

From a fabrication perspective, controlling film formation to ensure a uniform surface for PVSK growth is highly important in reducing propagation of defects, such as pinholes. Defects in the HTL can result in drops in the V_{oc} and shunt resistance and significant increases in series resistance. This is especially a challenge for the fabrication of NiO_x HTLs from nanoparticle solutions using blade coating or slot die coating, which to date have not surpassed spin-coated devices in performance. However, progress is being made and Yang et al. reported in 2022 a PCE of 19.87% on a fully blade coated flexible stack.[67] Thus developing methods to optimize the NiO_x/PVSK interface, improve film uniformity, control band alignment and conductivity are all active areas of NiO_x research.

While our focus is on nanoparticles, we would be remiss to ignore work that has been done with precursor deposition methods. Precursor deposition is a popular method for NiO_x film formation as it by passes the often-tedious cleaning process and directly forms the NiO_x film on the desired substrate. This has the advantage of being able to form highly uniform films with few defects.[73-77] However, this method has a high thermal cost (300-600 °C) and long annealing time (1-3 hours) that make it incompatible with flexible substrates. Work with photonic curing by Piper et al. has presented some promising results by reducing the annealing time to several seconds instead of hours.[77] However, there is still space for significant

development from their work as they were only able to produce devices with about 12% PCE. A recent example of work done using precursor inks, is the work of Li et al. with utilizing urea to passivate surface defects on the NiO_x surface. Their resulting devices achieved a champion PCE of 23.61% and a FF of 85.4%. While precursor-based inks have demonstrated remarkable efficiency, so to have nanoparticle-based inks without the high thermal cost. Our work has focused on moving to scalable deposition methods on flexible PET substrates so accounting for this high thermal cost has directed our current work to lower temperature options. An advantage of working with nanoparticles is the versatility they offer as composite coatings with other HTL materials or by functionalization of the particle surface. An active area of current research is in the passivation of defects at the NiO_x/PVSK interface. Whether by doping or introducing a passivator into the NiO_x ink prior to coating, nanoparticles can be customized to address the specific needs of the application.

The most common method for synthesizing NiO_x nanoparticles is the low temperature precipitation method.[64, 66, 69-72, 78, 79] In general a nickel salt is dissolved in water then precipitated by the addition of base to form $Ni(OH)_2$. The cleaned $Ni(OH)_2$ is then annealed at >270 °C to convert to the oxide, and suspended in water for coating. Controlling the particle surface through selection of the counter anions or introduction of ligands to the reaction mixture is critical for forming small, stable particles. In 2021, Guo et al. demonstrated an average 2% PCE increase when using nitrate vs chloride.[70] Their further analysis shows a direct relationship between ink stability and the identity of the initial counter anion. Addition of ligands prior to precipitation has also been shown to effectively control particle growth.[80] Cui et al. has taken this one step further by using alkylammonium hydroxides as the base to introduce alkylammonium ligands during precipitation.[66] The resulting particles were tuneable within a couple of nm in size and had a valence band maximum downshift of 0.26 eV. Their champion devices reached a PCE of 22%, with a duel NiO_x/PTAA HTL layer.

An alternative synthetic method, solvothermal synthesis, offers more control to the synthesis conditions. Usually centered around decomposing or reducing an oxygen containing metallo-organic salt, reactions are carried out at high temperatures and often in the presence of secondary reducing agents. The added control comes from the organics acting as coordinated ligands controlling particle growth.[81, 82] While solvothermal synthesis can provide control over particle morphology and properties, the poor atom economy, high energy costs and often poor yields make this synthesis route undesirable for larger applications and we discourage its use for future perovskite development.

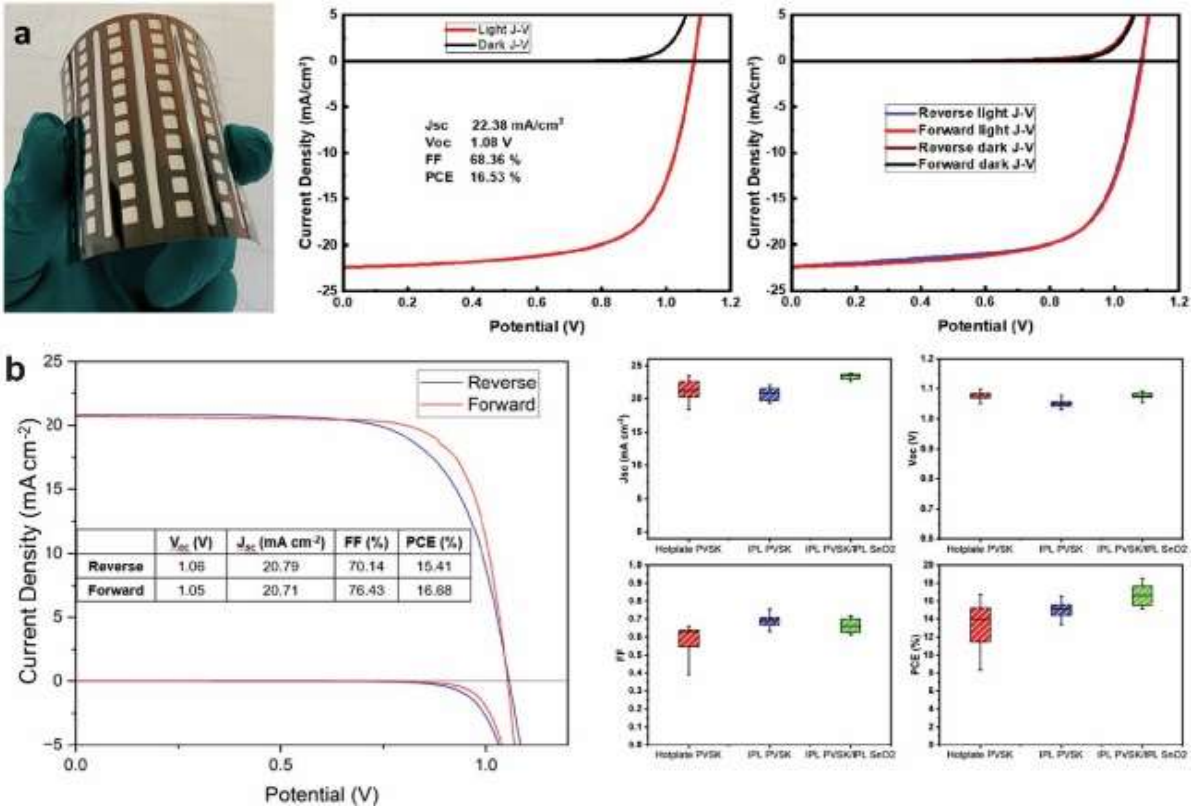

Figure 3: a) Image of flexible PSC and associated JV curve of champion p-i-n using solution processed SnO_2, with forward and reverse scan demonstrating low hysteresis. Reprinted (adapted) with permission from S. Chapagain, B. Martin, P. Armstrong, C. L. Perkins, M. O. Reese, T. Druffel and C. A. Grapperhaus, *ACS Appl. Mater.*, 2023, **6**, 4496-4502. Copyright 2023 American Chemical Society. b) JV curve of IPL annealed mixed cation perovskite and box plot showing effective IPL annealing of mixed cation perovskite and SnO_2. Reprinted (adapted) with permission from B. Martin, S. Chapagain, P. Armstrong, C. A. Grapperhaus, M. O. Reese and T. Druffel, *ACS Appl. Mater.*, 2023, DOI: 10.1021/acsaem.3c00134. Copyright 2023 American Chemical Society.

An additional property that is important to control in the particles during synthesis is the Ni^{2+}/Ni^{3+} ratio, which produces the innate p-type character of NiO_x.[63, 83-85] Doping with transition metals such as Co,[86] V,[87] and Cu,[69, 84] have been found to induce changes the Ni^{2+}/Ni^{3+} ratio while also improving conductivity.[85] A seminal investigation by Chen et al. in 2018 revealed important insights into the mechanism of Cu doping.[84] Utilizing DFT to calculate the density of states, they found a shift in gap state positions of NiO_x from 1.3 -2.0 eV to 0.7eV in Cu:NiO_x. This shift resulted in shallower acceptor levels which would likely lead to improvements in conductivity and the work function. Investigations by XPS showed no significant change in the Ni^{2+}/Ni^{3+} peak ratio, which was observed in prior studies, but did confirm the presence of both Cu^{2+} and Cu^{+} indicating that the change in conductivity is likely related to the copper oxidation state.[88] The exact mechanism for increasing conductivity from transition metal doping is still debated but studies like Zhang et al. on Li doped films in 2018 help to identify contributing features for alkali metal doping. They found that the addition of Li increased hole type carriers while shifting the valence band maximum towards the Fermi energy.[89]

While optimizing the ratio of Ni^{2+}/Ni^{3+} is important for high charge carrier density and conductivity, $Ni^{\geq 3+}$ at the PVSK interface has been found to induce device degradation. First reported by Boyd et al. in 2020, the presence of $Ni^{\geq 3+}$ sites at the film surface are highly reactive oxidants that can degrade the PVSK rapidly.[90] A similar report by Hsu et al. in 2020 also demonstrated this degradation by tracking reaction byproducts by MS-FTIR.[91] Boyd and Hsu both found that degradation is taking place through the A site cation with reactions being localized at the PVSK surface.

Our work to date has focused on developing ligands for stabilizing NiO_x in non-aqueous solvents such as chlorobenzene. This work took inspiration from studies by Liang et al. and Liu et al., both of which utilized long chain carboxylic acids with varying success.[81, 92] Starting from a solvothermal synthesis, we selected long alkyl chains functionalized with xanthates with the target of creating a micellular environment for the NiO_x particles. We found instead that we were able to stabilize the NiO_x particles by the addition of triethylamine and ethanol with mild heating (Figure 4). While effective at stabilizing our particles as dispersions in non-aqueous solvents, we were unable to produce functional devices of n-i-p configuration due to passivation of the PVSK surface that hindered charge extraction.[93] When deposited in the p-i-n configuration, device performances up to 14.47% PCE were obtained. Our current work is looking at further NiO_x formulations with a focus on optimizing interfacial compatibility. As such, we are exploring the effects of doping and interfacial passivation.

To date spin-coated films have made up the majority of NiO_x coatings (Table 2).[64, 94-98] While spin-coating is effective at forming uniform coatings, this method limits scalability and the results are often difficult to translate to larger area deposition methods.[46]. Other methods being explored are spray pyrolysis,[76] blade/meniscus coating,[67, 93, 99] and slot die roll to roll.[100] Our work has been exclusively centered on blade coating films. We have found film uniformity is significantly affected by the particle composition as that will in turn effect annealing conditions and interface defects. An example of this is seen in Figure 5 where we observed changes in film morphology based on particles composition.

While annealing free devices have been known for decades using particles prepared by precipitation, the addition of ligands or solvothermal based ligands require thermal annealing following deposition.[68, 69, 72, 101, 102] Annealing plays an important role in controlling the Ni^{2+}/Ni^{3+} ratio. One drawback of the post treatment free approach is the lack of control of this ratio. To address this challenge, the use of UV-O_3 post treatment is being explored in solgel systems.[87, 103, 104] In 2017 Islam et al. studied the effects of UV-O_3 treatment on NiO_x films in which they analyzed the change in resistance and XPS peak intensity in relation to treatment duration. They found 10-fold reduction in resistance after 10 min of UV-O_3 treatment, then 10-fold again after 60 min of treatment. They also reported a significant shift in the Ni^{2+}/Ni^{3+} ratio with increasing Ni^{3+} species found. Using glancing angle XPS they identified that the Ni^{3+} is predominantly generated at the film surface, but that it penetrates the film bulk as well.[103] Taking note of these results and applying similar methods to nanoparticles based films could be advantages for continued improvements. To date our reported work has been restricted to high thermal treatments due to the high temperature anneal that was necessary to remove our supporting ligands.

The future of NiO_x nanoparticles is optimistic but is still facing several material and process challenges. First material challenge that needs to be addressed is improving film conductivity while not accelerating degrading of the perovskite by over exposure to Ni^{3+}. As discussed, doping has shown promise in addressing this issue but have fallen short with secondary organic passivators still required to improve device stability. There is significant space available for exploring particle ligands or passivator film design. To date incorporation of Lewis basic moieties such as amines and thiols has proven effective at coordinating to the NiO_x surface and providing a bridge to the perovskite. Furthermore, organic HTL's with internal molecular dipoles have shown to increase V_{oc} while reducing hysteresis.[105] Incorporating internal dipoles into material design could further improve the NiO_x/PVSK interface. If the nanoparticle ligands are designed to assist conductivity and fermi level alignment in addition to controlling particle size and ink stability, then removing ligands post deposition will not be necessary. This leads to the first process challenge, post process annealing. While conventional annealing is compatible with glass-based substrates, as flexible substrates and high throughput development expands, large ovens and high temperatures are less practical. Rapid annealing methods such as UV-ozone, ozone plasma, or IPL can create the highly oxidative environments necessary to achieve the desired increase in conductivity at shorter time scales.

Table 2: Survey of recent works using NiO_x as the HTL. SC: Spin-coating

Device architecture	HTL	Deposition	Processing	J_{sc}	V_{oc}	FF	PCE	Ref
Regular (P-I-N) architecture								
Glass/ ITO/ NiO_x-Urea/ $CsFAMAPbI_3$/ BzMIMBr/ C60/ BCP/ Ag	Precursor	Spray Pyrolysis	400C, 20 min	24.04	1.15	85.4	23.61	76
glass/ ITO/ NiO_x/ triple-cation perovskite/ $PC_{61}BM$/ ZnO NPs/ Ag	Precipitation, Precursor	SC	350C, 30 min or 300C, 45 min	24.34	1.06	79.18	20.45	106
Glass/ NiO_x/ CsFAMAPbIBr/ PCBM:C60/ BCP/ Au	Precipitation	SC	100C, 10 min	23.49	1.15	84.68	22.81	101
Glass/ ITO/ NiO_x/ PTAA/ CsFAMAPbIBr/ PCBM/ Ag	Precipitation	SC	150C, 20 min	24.52	1.13	82	22.71	66
Glass/ ITO/ NiO_x/ CsFAMAPbIBr/ C60/ BCP/ Cu	Precursor	SC	180C, 10 min+ 400C, 45 min or UV lamp 10min	24.25	1.126	82.19	22.45	104
Glass/ ITO/ NiO_x/ CBSA/ CsFAMAPbIBr/ PCBM/ BCP/ Ag	Precipitation	SC	130C, 20 min	23.72	1.11	81.43	21.8	107
Glass/ ITO/ NiO_x/ TMPA/ MAPbI/ PCBM/ BCP/ Ag	Precipitated	SC	No Anneal	23.7	1.07	80.4	20.4	102
PEN/ hc-PEDOT:PSS/ NiO_x/ $Cs_{0.05}FA_{0.85}MA_{0.10}Pb(I_{0.97}Br_{0.03})_3$/ PCBM/ Ag	Precipitation	Blade Coated	130 C, 30 min	23.74	1.12	74.7	19.87	67
Glass/ ITO/ Li:NiO_x/ NiO_x/ FAMAPbIBr/ PCBM/ BCP/ Ag	Precursor	SC	120 C, 10 min + 2nd coat 450 C, 1h	23.22	0.99	82.83	19.04	74
Glass/ ITO/ V:NiO_x/ $MAPbI_3$/ PCBM/ BCP/ Ag	Solvothermal	SC	25C, 15 min + UV-V 20 min	19.81	1.04	75	15.45	87
Glass or PET/ ITO/ NiO_x/ $MAPbI_{3-x}Cl_x$ / PCBM-C60/ Zracac/ Ag	Precipitation	SC	No Anneal	23.16/ 22.02	1.11/ 1.06	81/ 78	20.83/ 18.16	69
Glass/ ITO/ NiO_x/ $Cs_{0.05}MA_{0.16}FA_{0.79}Pb_{1.03}(Br_{0.16}I_{0.86})_3$/ LiF/ C60/ BCP/ Ag	Precursor, Sputtered, Precipitation	SC	Precursor: 400C, 50 min; Nanoparticles: No Anneal	19.56	1.15	84.7	19.06	90
Inverted(N-I-P) architecture								
Glass/ ITO/ TiO_2/ MAPbI/ NiO_x/ Au	Precipitation	SC	100C, 5 min	23.59	0.885	60.1	12.57	78

The annealing challenge is further compounded when looking to apply NiO_x in the n-i-p configuration, another material challenge. While p-i-n is the default stack for NiO_x, there are some examples with an inverted n-i-p stack. To date, effective devices have only been demonstrated using vacuum methods such as sputtering or thermal evaporation to deposit NiO_x on top of the PVSK layer. Attempts utilizing long chain ligands to disperse NiO_x in PVSK compatible organic solvents have failed to result in high performing devices with best champion device reported by Pirzad et al. with a champion PCE of 12.6%. In that study, they were unable to get higher efficiency due to low V_{oc} (0.88V) and FF (60%) that resulted from the incorporation of oleic acid in their ink formulation.[78] Instead of trying to suspend the extremely hydrophilic NiO_x in chlorobenzene based

Figure 4. Reaction scheme demonstrating the functionalization of synthesized NiO_x nanoparticles with xanthate ligands and dispersion into chlorobenzene solutions. Used with permission of Nanotechnology, from "Solvation of NiO_x for hole transport layer deposition in perovskite solar cells." Armstrong, P. J., et al 33(6), (2021); permission conveyed through Copyright Clearance Center, Inc

solutions, we propose looking at more polar options such as short chain alcohols. Based on our work with SnO_2, short chain alcohols have been shown to be compatible with the PVSK surface and would require significantly shorter ligands to successfully suspend NiO_x.

Transitioning away from spin coating to more scalable methods, like slot die coating, present a significant process challenge. Nanoparticles have a distinct advantage over traditional precursor inks when deposited at scale in that they have a lower thermal requirement for post deposition annealing. Particles with low or no annealing requirements are ideal for large scale flexible coatings but this is dependent on ink formulation. Current ink formulations are aqueous suspensions with particles stabilized electrostatically. This formulation is effective for spin coating but presents severe wetting issues when taken to large area coatings or high-speed coatings. Inks need to be formulated with surface wetting, and film drying in mind as well as particle stability. Like our suggestion for developing inks for n-i-p, we recommend looking into short chain alcohol for high wetting and fast drying solvents. The addition of ligands to the particle matrix needs to be done with caution as they directly affect the packing dynamics of the particles and are hard to remove once coated on flexible substrates. For this reason, we recommend the use of interfacial passivator films to address uniformity issues and initial particle size control over the inclusion of current common ligands or surfactants. Despite the shortcoming listed here NiO_x is the material best suited for large, scaled roll out.

2.3 Encapsulation

Perovskite solar cells are sensitive to moisture, oxygen, temperature, and UV. To overcome these problems, encapsulation is often utilized. Encapsulation protects the solar cell by creating a barrier that delays contact between the ambient air and cells.[108] There are various types of encapsulation techniques that have been developed to improve the stability of PSCs under humid conditions. These include glue-based lab encapsulation, lamination-based COM encapsulation, and thin film encapsulation.[109, 110]

Thin film encapsulation are thin compact hydrophobic coatings traditionally composed of hydrophobic polymers. They are considered the most promising encapsulation method for flexible devices. Thin film encapsulants are light weight, flexible, cost effective, and can be compatible with roll-to-roll manufacturing. They can be used in portable and wearable devices too.

In a recent study of thin film encapsulation, Han et al. reported on the effect of poly(methyl-methacrylate) PMMA/reduced graphene oxide (rGO) composite as a passivation layer. The interaction of hydrophilic rGO and hydrophobic PMMA polymer created a hydrophobic surface that hinders the diffusion path of H_2O, O_2, and other gases into the PVSK.[111, 112] Jang et al., used two fillers, SiO_2 and graphene oxide (GO) in poly(vinyl-co-ethylene) EVOH to decrease moisture penetration. A UV-treatment of SiO_2 helped to increase its dispersion in the precursor solution, while the use of EVOH made the penetration

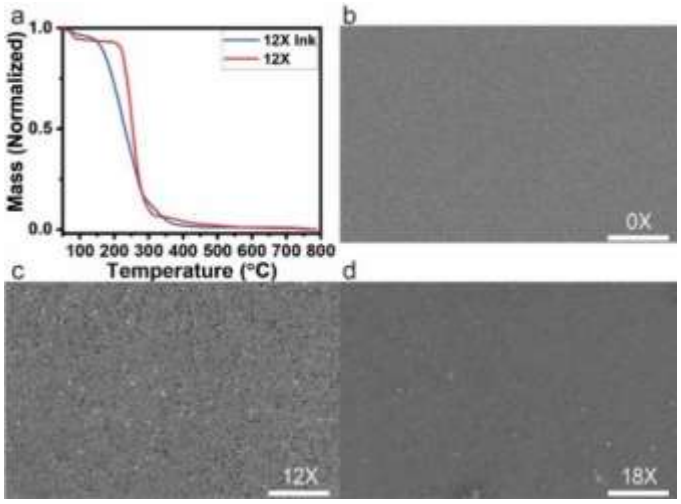

Figure 5. a) TGA of 12X ligand as a solid and the 12X ink as a thick film confirming degradation of the xanthate at temperatures above 300 °C. b-d) SEM images of 0X, 12X, and 18X films prepared by blade coating showing changes in film uniformity in the presence of xanthate ligands. Scale bars are 5 µm. Used with permission of Nanotechnology, from "Solvation of NiO_x for hole transport layer deposition in perovskite solar cells." Armstrong, P. J., et al 33(6), (2021); permission conveyed through Copyright Clearance Center, Inc.

path of water more intricate. This decreased the water vapor transmission rate (WVTR) value to 1.55 x 10^2 g/m^{2}day from 4.72 x 10^{-2} g/m^{2}day. Moreover, the addition of GO decreased the hydroxyl groups on the surface of EVOH thus decreasing its hydrophilicity. Utilizing both fillers, GO and SiO_2 in EVOH further improves the WVTR value to 3.34 x 10^{-3} g/m^{2}day.[113]

Our group has explored the use of graphene/polyaniline (PANI) composite as an encapsulating coating. We compared stability and performance of devices with graphene/PANI composite with devices having only multi-functional graphene or PANI. To test PVSK stability, samples were monitored by PXRD after aging in the presence of 99% RH air for 2 days. No degradation was observed in the graphene/PANI composite sample. When PANI was used alone there was complete loss of the PVSK peaks and the appearance of the peak at 12.6° indicating PbI_2 formation. When graphene was used alone, there was a decrease in peak intensity for the PVSK and the appearance of graphene peaks as shown in Figure 6a indicating some degradation but not complete decomposition.

Investigating the effect on current density-voltage curves showed a rapid decline in the J_{sc} and V_{oc} in unencapsulated samples. After 1 hour no photovoltaic behavior was observed. In encapsulated samples we found that by coating a 2-4 µm thick layer degradation was stopped. By repeating the spin-coated depositions, the thickness of the coated film could be tuned. When comparing thickness of the encapsulation layer, stability was found to improve with thickness. This is because film thickness increases the tortuosity of the diffusion path by which water molecules enter the PVSK and causes degradation as shown in Figure 6b. [114]

Looking at materials that could be used in the future, graphene oxide or fullerenes composited with other carbon nanomaterials like carbon nanotubes (CNTs) and carbon black hold promise. In a CNT/graphene composite CNTs would act as reinforcement agents to provide the ink with mechanical

strength, meanwhile the exceptional barrier properties and high transparency of graphene oxide help to enhance the overall performance and stability of the encapsulated PVSK solar cells. Similarly, graphene oxide with carbon black composite could be another good encapsulant for PSCs. Carbon black is a highly conductive and stable carbon nanomaterial. Carbon black particles well dispersed within the graphene oxide matrix would improve the electrical properties and enhance the overall stability of the PVSK solar cell. The value of improving the electrical properties of the encapsulation lies in replacing the back contact electrode and having a dual-purpose electrode/encapsulation layer. The deposition of graphene oxide-based composites by blade coating could help remove vacuum processing steps from current fabrication methods This would reduce material costs and processing steps for PSCs manufacturing.

Further improvement of barrier properties could be achieved by incorporating inorganic NPs or a mixture of NPs with hydrophobic polymers. Inorganic nanomaterials with good barrier properties such as SiO_2, TiO_2, and Al_2O_3 have lower values of WVTR and oxygen transmission rate.

To date thin film encapsulates have been deposited by spin coating. Due to their solution processibility they are compatible with scalable processes like blade coating, inkjet printing, etc.

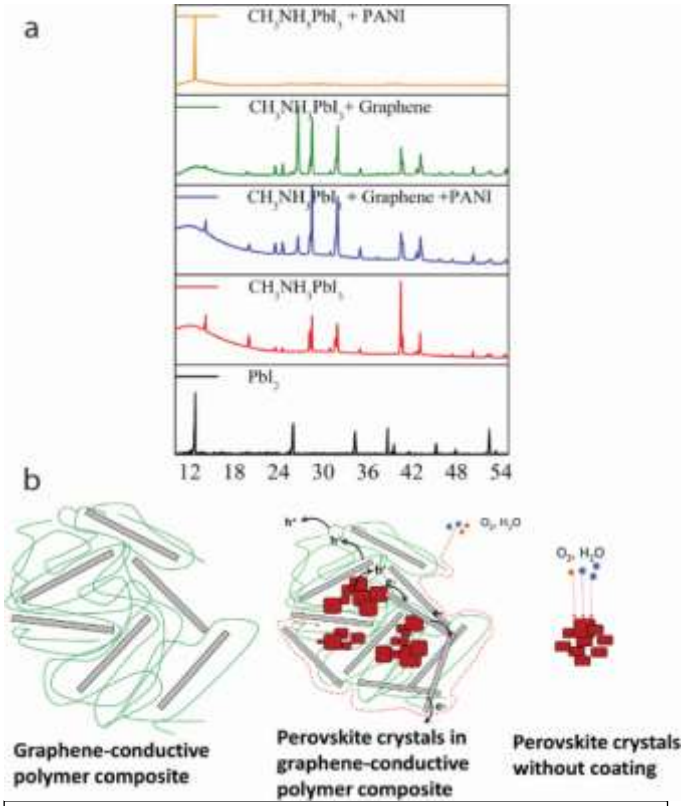

Figure 6: a) XRD pattern of pristine PbI_2, unprotected $MAPbI_3$, graphene and PANI protected $MAPbI_3$, $MAPbI_3$ with graphene and $MAPbI_3$ with PANI (b) The graphene-conductive polymer composite. The tortuous path of oxygen and water molecules to reach the perovskite and the direct transport path of water and air molecules towards unprotected perovskite crystals. Used with permission of Nanotechnology, from "Stable and durable $CH_3NH_3PbI_3$ perovskite solar cells at ambient conditions" Nagalingam Rajamanickam *et al* **27** 235404 (2016); permission conveyed through Copyright Clearance Center, Inc.

As a result, the transition from laboratory scale to large industrial scale production appears promising in the future.

3.0 Summary and Future Perspective

Nanoparticles are an ideal material candidate for the CTL layers for a perovskite device based on their scalability, formulation control and aligned optoelectronic properties as demonstrated in this review article. The utility of nanoparticles in several layers of a PVSK device have been discussed in this feature article. Specifically, SnO_2 and NiO_x nanoparticles were discussed at length as charge transport layers due to their suitable band alignments, charge carrier mobilities and stability. A variety of synthetic methods are discussed for each material in relation to ink formulation and device performance. The versatility of nanoparticles provides significant opportunity for doping and ligand design to further improve the electronic properties and particle stability. These materials have also been discussed in the context of material scalability with emphasis being placed on blade coating and slot die coating methods. Also reviewed, is the use of carbonaceous composite encapsulation layers as solution processed thin film encapsulate in PSCs.

SnO_2 inks have been demonstrated with yttrium doping and functionalization for deposition directly onto a PVSK film, yielding a functional device of over 16%. Device performance can be further improved with continued research in doping or annealing of films. However, with moving to the top PVSK surface there are several new challenges that need to be addressed. Traditional hotplate and thermal annealing are ineffective at sintering SnO_2 particles without degrading the perovskite when coated as a top layer. Alternative rapid annealing methods like IPL should be explored. Additionally, packing of nanoparticles with low or no annealing is prone to film porosity. This could also be addressed through sintering or the development of a suitable interfacial coating.

NiO_x has demonstrated itself as a highly effective HTL with wide application in p-i-n architectures and spin coating applications. Transitioning NiO_x to wide area deposition methods still presents several significant challenges in ink stability and post annealing. A more in depth understanding of the NiO_x particle surface and reactive sites would aid in developing affective ligands that can assist in particle stability while not interfering with charge extraction once deposited. This could also be essential to successfully depositing a solution phase NiO_x as the top HTL in a n-i-p architecture. Concurrently developing passivating interfacial materials that both improve band alignment while reducing Ni^{3+} induced degradation of the perovskite holds significant research opportunities.

In total, current research has focused on developing high performance devices and has found that earth abundant materials like SnO_2 and NiO_x are strong candidates for CTL's in PSCs. Both nanoparticle and precursor ink formulations have been explored extensively with heavy emphasis being focused on device performance. Annealing of CTLs on top of the perovskite is a special challenge. We have demonstrated the use of IPL with metal oxide thin films that are deposited either under the PVSK or on top and utilize the thermal response from

the PVSK to further anneal the metal oxides. Further work with IPL or other rapid annealing methods will be necessary to properly sinter metal oxides films coated on top of perovskite films. Unless such methods are developed nanoparticle inks are preferential to precursor inks. Processing of CTL thin films by scalable methods is still in need of significant research for them to reach the same performances as traditional laboratory methods.

Author Contributions

Writing done by Peter Armstrong, Sashil Chapagain, Rojita Panta. Supervised by Craig Grapperhaus, and Thad Druffel

Conflicts of interest

There are no conflicts to declare.

Acknowledgements

The authors would like to thank the Conn Center for Renewable Energy Research and Micro/Nano Technology Center at the University of Louisville for assisting in the characterization of our work. This work is funded in part or whole by the U.S.Department of Energy Solar Energy Technologies Office AwardNumber(s) DE-EE0008752

Notes and references

1. N. R. E. Laboratory, Best Research-Cell Efficiency Chart, https://www.nrel.gov/pv/cell-efficiency.html, (accessed 8-8-23, 2023).
2. M. A. Green, E. D. Dunlop, G. Siefer, M. Yoshita, N. Kopidakis, K. Bothe and X. Hao, *Prog. Photovolt.: Res. Appl.*, 2022, **31**, 3-16.
3. Z. Xu, Q. Zhuang, Y. Zhou, S. Lu, X. Wang, W. Cai and Z. Zang, *Small Structures*, 2023, **n/a**, 2200338.
4. Z. Wu, W. Li, Y. Ye, X. Li and H. Lin, *Sustain. Energy. Fuels*, 2021, **5**, 1926-1951.
5. Z. Li, T. R. Klein, D. H. Kim, M. Yang, J. J. Berry, M. F. A. M. van Hest and K. Zhu, *Nat. Rev. Mater*, 2018, **3**, 18017.
6. J. Yang, E. L. Lim, L. Tan and Z. Wei, *Adv. Energy Mater.*, 2022, **12**, 2200975.
7. H. Choi, K. Choi, Y. Choi, T. Kim, S. Lim and T. Park, *Small Methods*, 2019, **4**.
8. J. Yun, J. Jun, H. Yu, K. Lee, J. Ryu, J. Lee and J. Jang, *J. Mater. Chem. A*, 2017, **5**, 21750-21756.
9. Z. Liu, T. He, K. Liu, J. Wang, Y. Zhou, J. Yang, H. Liu, Y. Jiang, H. Ma and M. Yuan, *J. Mater. Chem. A*, 2017, **5**, 24282-24291.
10. N. Besra, K. Sardar, S. Maiti, P. K. Sarkar, T. Paul, S. Thakur, G. Majumdar and K. K. Chattopadhyay, *Dalton Transactions*, 2020, **49**, 15788-15799.
11. S. Ahmad, H. Abbas, M. Bilal Khan, V. Nagal, A. K. Hafiz and Z. H. Khan, *Sol. Energy*, 2021, **216**, 164-170.
12. S. Chapagain, B. Martin, P. Armstrong, C. L. Perkins, M. O. Reese, T. Druffel and C. A. Grapperhaus, *ACS Appl. Mater.*, 2023, **6**, 4496-4502.
13. Q. Jiang, Y. Zhao, X. Zhang, X. Yang, Y. Chen, Z. Chu, Q. Ye, X. Li, Z. Yin and J. You, *Nat. Photonics*, 2019, **13**, 460-466.
14. L. Current status of electronYang, Q. Xiong, Y. Li, P. Gao, B. Xu, H. Lin, X. Li and T. Miyasaka, *J. Mater. Chem. A*, 2021, **9**, 1574-1582.
15. K. Mahmood, S. Sarwar and M. T. Mehran, *RSC Adv.*, 2017, **7**, 17044-17062.
16. Y. Zhou, X. Li and H. Lin, *Small*, 2020, **16**, 1902579.
17. L. Lin, T. W. Jones, T. C. J. Yang, N. W. Duffy, J. Li, L. Zhao, B. Chi, X. Wang and G. J. Wilson, *Adv. Funct. Mater.*, 2021, **31**, 2008300.
18. J. Tsiba Matondo, D. Malouangou Maurice, Q. Chen, L. Bai and M. Guli, *Sol. Energ. Mat. Sol. C.*, 2021, **224**, 111011.
19. A. Bouich, J. C. Torres, H. Chfii, J. Marí-Guaita, Y. H. Khattak, F. Baig, B. M. Soucase and P. Palacios, *Sol. Energy*, 2023, **250**, 18-32.
20. L. J. Sutherland, H. C. Weerasinghe and G. P. Simon, *Adv. Energy Mater.*, 2021, **11**, 2101383.
21. E. Muchuweni, B. S. Martincigh and V. O. Nyamori, *Adv. Energy Sustainability Res.*, 2021, **2**, 2100050.
22. A. Kojima, K. Teshima, Y. Shirai and T. Miyasaka, *J. Am. Chem. Soc.*, 2009, **131**, 6050-6051.
23. J. M. Ball, M. M. Lee, A. Hey and H. J. Snaith, *Energ. Environ. Sci.*, 2013, **6**, 1739-1743.
24. M. Liu, M. B. Johnston and H. J. Snaith, *Nature*, 2013, **501**, 395-398.
25. H. Min, D. Y. Lee, J. Kim, G. Kim, K. S. Lee, J. Kim, M. J. Paik, Y. K. Kim, K. S. Kim and M. G. Kim, *Nature*, 2021, **598**, 444-450.
26. L. Xiong, Y. Guo, J. Wen, H. Liu, G. Yang, P. Qin and G. Fang, *Adv. Funct. Mater.*, 2018, **28**, 1802757.
27. T. Leijtens, G. E. Eperon, S. Pathak, A. Abate, M. M. Lee and H. J. Snaith, *Nat. Commun.*, 2013, **4**, 2885.
28. J. Yang, B. D. Siempelkamp, E. Mosconi, F. De Angelis and T. L. Kelly, *Chem. Mater.*, 2015, **27**, 4229-4236.
29. L. L. Deng, S. Y. Xie and F. Gao, *Adv. Electron. Mater.*, 2018, **4**, 1700435.
30. C. Ran, Y. Chen, W. Gao, M. Wang and L. Dai, *J. Mater. Chem. A*, 2016, **4**, 8566-8572.
31. S. Shao, M. Abdu-Aguye, L. Qiu, L.-H. Lai, J. Liu, S. Adjokatse, F. Jahani, M. E. Kamminga, G. H. ten Brink and T. T. Palstra, *Energ. Environ. Sci.*, 2016, **9**, 2444-2452.
32. S. Y. Park, M. Y. Baek, Y. Ju, D. H. Kim, C. S. Moon, J. H. Noh and H. S. Jung, *J. Phys. Chem. Lett.*, 2018, **9**, 5460-5467.
33. H. Xie, X. Yin, P. Chen, J. Liu, C. Yang, W. Que and G. Wang, *Mater. Lett.*, 2019, **234**, 311-314.
34. J. Song, E. Zheng, J. Bian, X.-F. Wang, W. Tian, Y. Sanehira and T. Miyasaka, *J. Mater. Chem. A*, 2015, **3**, 10837-10844.
35. Q. Jiang, L. Zhang, H. Wang, X. Yang, J. Meng, H. Liu, Z. Yin, J. Wu, X. Zhang and J. You, *Nat. Energy*, 2016, **2**, 1-7.
36. Q. Jiang, Z. Chu, P. Wang, X. Yang, H. Liu, Y. Wang, Z. Yin, J. Wu, X. Zhang and J. You, *Adv. Mater.*, 2017, **29**, 1703852.
37. G. Yang, C. Chen, F. Yao, Z. Chen, Q. Zhang, X. Zheng, J. Ma, H. Lei, P. Qin and L. Xiong, *Adv. Mater.*, 2018, **30**, 1706023.
38. A. C. Bose, D. Kalpana, P. Thangadurai and S. Ramasamy, *J. Power Sources*, 2002, **107**, 138-141.
39. Y. W. Noh, J. H. Lee, I. S. Jin, S. H. Park and J. W. Jung, *Nano Energy*, 2019, **65**, 104014.

40. Y. Bai, Y. Fang, Y. Deng, Q. Wang, J. Zhao, X. Zheng, Y. Zhang and J. Huang, *ChemSusChem*, 2016, **9**, 2686-2691.
41. P. S. Chandrasekhar, S. Chapagain, M. Blake, P. J. Armstrong, C. Grapperhaus and T. L. Druffel, *Sustain. Energy. Fuels*, 2022, **6**, 5316-5323.
42. B. Dou, J. B. Whitaker, K. Bruening, D. T. Moore, L. M. Wheeler, J. Ryter, N. J. Breslin, J. J. Berry, S. M. Garner and F. S. Barnes, *ACS Energy Lett.*, 2018, **3**, 2558-2565.
43. Y. Wang, L. Yang, C. Dall'Agnese, G. Chen, A.-J. Li and X.-F. Wang, *Front. Chem. Sci. Eng.*, 2021, **15**, 180-186.
44. J. You, L. Meng, T.-B. Song, T.-F. Guo, Y. Yang, W.-H. Chang, Z. Hong, H. Chen, H. Zhou and Q. Chen, *Nat. Nanotechnol.*, 2016, **11**, 75-81.
45. S. Chapagain, P. S. Chandrasekhar, D. McGott, R. C. Bramante, M. F. van Hest, M. O. Reese, T. Druffel and C. A. Grapperhaus, *ACS Appl. Energy Mater.*, 2021, **4**, 10477-10483.
46. B. Martin, S. Chapagain, P. Armstrong, C. A. Grapperhaus, M. O. Reese and T. Druffel, *ACS Appl. Mater.*, 2023, **6**, 5207-5216.
47. M. Park, J.-Y. Kim, H. J. Son, C.-H. Lee, S. S. Jang and M. J. Ko, *Nat. Energy*, 2016, **26**, 208-215.
48. H. Ye, Z. Liu, X. Liu, B. Sun, X. Tan, Y. Tu, T. Shi, Z. Tang and G. Liao, *Appl. Surf. Sci.*, 2019, **478**, 417-425.
49. X. Ren, D. Yang, Z. Yang, J. Feng, X. Zhu, J. Niu, Y. Liu, W. Zhao and S. F. Liu, *ACS Appl. Mater. Interfaces*, 2017, **9**, 2421-2429.
50. B.-X. Chen, H.-S. Rao, W.-G. Li, Y.-F. Xu, H.-Y. Chen, D.-B. Kuang and C.-Y. Su, *J. Mater. Chem. A*, 2016, **4**, 5647-5653.
51. Y. Lv, B. Cai, Q. Ma, Z. Wang, J. J. Liu and W.-H. Zhang, *RSC Adv.*, 2018, **8**, 20982-20989.
52. G. Yang, H. Lei, H. Tao, X. Zheng, J. Ma, Q. Liu, W. Ke, Z. Chen, L. Xiong and P. Qin, *Small*, 2017, **13**, 1601769.
53. M. Degani, Q. An, M. Albaladejo-Siguan, Y. J. Hofstetter, C. Cho, F. Paulus, G. Grancini and Y. Vaynzof, *Sci. Adv.*, 2021, **7**, eabj7930.
54. J. J. Yoo, G. Seo, M. R. Chua, T. G. Park, Y. Lu, F. Rotermund, Y.-K. Kim, C. S. Moon, N. J. Jeon and J.-P. Correa-Baena, *Nature*, 2021, **590**, 587-593.
55. M. Kim, J. Jeong, H. Lu, T. K. Lee, F. T. Eickemeyer, Y. Liu, I. W. Choi, S. J. Choi, Y. Jo and H.-B. Kim, *Science*, 2022, **375**, 302-306.
56. S. Siegrist, P. Nandi, R. K. Kothandaraman, A. Abdessalem, A. N. Tiwari and F. Fu, *Sol. RRL*, 2023, DOI: 10.1002/solr.202300273.
57. T. Bu, J. Li, F. Zheng, W. Chen, X. Wen, Z. Ku, Y. Peng, J. Zhong, Y.-B. Cheng and F. Huang, *Nat. Commun.*, 2018, **9**, 4609.
58. B. Taheri, F. De Rossi, G. Lucarelli, L. A. Castriotta, A. Di Carlo, T. M. Brown and F. Brunetti, *ACS Appl. Mater.*, 2021, **4**, 4507-4518.
59. A. H. Ghahremani, D. Ratnayake, A. Sherehiy, D. O. Popa and T. Druffel, *Energ. Technol.*, 2021, **9**, 2100452.
60. J. Tirado, M. Vásquez-Montoya, C. Roldán-Carmona, M. Ralaiarisoa, N. Koch, M. K. Nazeeruddin and F. Jaramillo, *ACS Appl. Mater.*, 2019, **2**, 4890-4899.
61. Y. Wang, C. Duan, J. Li, W. Han, M. Zhao, L. Yao, Y. Wang, C. Yan and T. Jiu, *ACS Appl. Mater. Interfaces*, 2018, **10**, 20128-20135.
62. C. H. Teh, R. Daik, E. L. Lim, C. C. Yap, M. A. Ibrahim, N. A. Ludin, K. Sopian and M. A. Mat Teridi, *J. Mater. Chem. A*, 2016, **4**, 15788-15822.
63. Q. Wang, Z. Lin, J. Su, Z. Hu, J. Chang and Y. Hao, *Nano Select*, 2021, **2**, 1055-1080.
64. H. Zhang, C. Zhao, J. Yao and W. C. H. Choy, *Angew. Chem., Int. ED*, 2023, **n/a**, e202219307.
65. S. Pitchaiya, M. Natarajan, A. Santhanam, V. Asokan, A. Yuvapragasam, V. Madurai Ramakrishnan, S. E. Palanisamy, S. Sundaram and D. Velauthapillai, *Arab. J. Chem.*, 2020, **13**, 2526-2557.
66. X. Cui, J. Jin, J. Zou, Q. Tang, Y. Ai, X. Zhang, Z. Wang, Y. Zhou, Z. Zhu, G. Tang, Q. Cao, S. Liu, X. Liu and Q. Tai, *Adv. Funct. Mater.*, 2022, **32**, 2203049.
67. X. Yang, H. Yang, M. Su, J. Zhao, X. Meng, X. Hu, T. Xue, Z. Huang, Y. Lu, Y. Li and Z. Yang, *Sol. RRL*, 2022, **6**, 2100991.
68. H. Zhang, J. Cheng, F. Lin, H. He, J. Mao, K. S. Wong, A. K. Y. Jen and W. C. H. Choy, *ACS Nano*, 2016, **10**, 1503-1511.
69. D. Ouyang, J. Zheng, Z. Huang, L. Zhu and W. C. H. Choy, *J. Mater. Chem. A*, 2021, **9**, 371-379.
70. T. Guo, Z. Zhang, L. Yu, H. Yuan, J. Zhang, X. Liu, Z. Hu and Y. Zhu, *Journal of Alloys and Compounds*, 2021, **860**.
71. S. Bai, P. Da, C. Li, Z. Wang, Z. Yuan, F. Fu, M. Kawecki, X. Liu, N. Sakai, J. T.-W. Wang, S. Huettner, S. Buecheler, M. Fahlman, F. Gao and H. J. Snaith, *Nature*, 2019, **571**, 245-250.
72. F. Jiang, W. C. H. Choy, X. Li, D. Zhang and J. Cheng, *Adv. Mater.*, 2015, **27**, 2930-2937.
73. M. Li, X. Xu, Y. Xie, H.-W. Li, Y. Ma, Y. Cheng and S.-W. Tsang, *J. Mater. Chem. A*, 2019, **7**, 9578-9586.
74. L. Zhao, X. Sun, Q. Yao, S. Huang, L. Zhu, J. Song, Y. Zhao and Y. Qiang, *Advanced Materials Interfaces*, 2022, **9**, 2101562.
75. X. Zhang, L. Shen, P. Baral, S. N. Vijayaraghavan, F. Yan, X. Gong and H. Wang, *Sol. Energ. Mat. Sol. C.*, 2022, **246**, 111894.
76. C. Li, Y. Zhang, X. Zhang, P. Zhang, X. Yang and H. Chen, *Adv. Funct. Mater.*, 2023, **33**, 2214774.
77. R. T. Piper, T. B. Daunis, W. Xu, K. A. Schroder and J. W. P. Hsu, *Frontiers in Energy Research*, 2021, **9**.
78. S. Pirzad Ghias Abadi, M. Borhani Zarandi and N. Jahanbakhshi Zadeh, *Synthetic Metals*, 2022, **289**.
79. J. Ciro, D. Ramírez, M. A. Mejía Escobar, J. F. Montoya, S. Mesa, R. Betancur and F. Jaramillo, *ACS Appl. Mater. Interfaces*, 2017, **9**, 12348-12354.
80. Y. Bahari Molla Mahaleh, S. K. Sadrnezhaad and D. Hosseini, *Journal of Nanomaterials*, 2008, **2008**, 470595.
81. X. Liang, Q. Yi, S. Bai, X. Dai, X. Wang, Z. Ye, F. Gao, F. Zhang, B. Sun and Y. Jin, *Nano Lett.*, 2014, **14**, 3117-3123.
82. E. R. Beach, K. Shqau, S. E. Brown, S. J. Rozeveld and P. A. Morris, *Mater. Chem. Phys.*, 2009, **115**, 371-377.
83. S. S. Shin, S. J. Lee and S. I. Seok, *Adv. Funct. Mater.*, 2019, **29**, 1900455.
84. W. Chen, Y. Wu, J. Fan, A. B. Djurišić, F. Liu, H. W. Tam, A. Ng, C. Surya, W. K. Chan, D. Wang and Z.-B. He, *Adv. Energy Mater.*, 2018, **8**, 1703519.
85. D. Di Girolamo, F. Di Giacomo, F. Matteocci, A. G. Marrani, D. Dini and A. Abate, *Chem. Sci.*, 2020, **11**, 7746-7759.
86. Z. R. Marand, A. Kermanpur, F. Karimzadeh, E. M. Barea, E. Hassanabadi, E. H. Anaraki, B. Julián-López, S. Masi and I. Mora-Seró, *Nanomaterials*, 2020, **10**, 872.
87. A. Kotta, I. Seo, H.-S. Shin and H.-K. Seo, *Chem. Eng. J.*, 2022, **435**, 134805.
88. X. Xu, H. Zhang, Y. Tong, Y. Sun, X. Fang, J. Xu and X. Wang, *Applied Surface Science*, 2021, **550**, 149316.

89. J. Y. Zhang, W. W. Li, R. L. Z. Hoye, J. L. MacManus-Driscoll, M. Budde, O. Bierwagen, L. Wang, Y. Du, M. J. Wahila, L. F. J. Piper, T. L. Lee, H. J. Edwards, V. R. Dhanak and K. H. L. Zhang, *J. Mater. Chem. C*, 2018, **6**, 2275-2282.
90. C. C. Boyd, R. C. Shallcross, T. Moot, R. Kerner, L. Bertoluzzi, A. Onno, S. Kavadiya, C. Chosy, E. J. Wolf, J. Werner, J. A. Raiford, C. de Paula, A. F. Palmstrom, Z. J. Yu, J. J. Berry, S. F. Bent, Z. C. Holman, J. M. Luther, E. L. Ratcliff, N. R. Armstrong and M. D. McGehee, *Joule*, 2020, **4**, 1759-1775.
91. S. Thampy, B. Zhang, K.-H. Hong, K. Cho and J. W. P. Hsu, *ACS Energy Lett.*, 2020, **5**, 1147-1152.
92. Z. Liu, A. Zhu, F. Cai, L. Tao, Y. Zhou, Z. Zhao, Q. Chen, Y.-B. Cheng and H. Zhou, *J. Mater. Chem. A*, 2017, **5**, 6597-6605.
93. P. J. Armstrong, P. S. Chandrasekhar, S. Chapagain, C. M. Cline, M. F. A. M. van Hest, T. Druffel and C. A. Grapperhaus, *Nanotechnology*, 2021, **33**, 065403.
94. A. J and T. Sahoo, *Materials Research Express*, 2020, **7**, 016405.
95. S.-K. Kim, H.-J. Seok, D.-H. Kim, D.-H. Choi, S.-J. Nam, S.-C. Kim and H.-K. Kim, *RSC Adv.*, 2020, **10**, 43847-43852.
96. S.-H. Huang, C.-K. Guan, P.-H. Lee, H.-C. Huang, C.-F. Li, Y.-C. Huang and W.-F. Su, *Adv. Energy Mater.*, 2020, **10**, 2001567.
97. K. C. Icli and M. Ozenbas, *Electrochim. Acta*, 2018, **263**, 338-345.
98. M. Y. Woo, K. Choi, J. H. Lee, S. Y. Park and J. H. Noh, *Adv. Energy Mater.*, 2021, **n/a**, 2003119.
99. C. Wu, Y. Huang, S. Wang, X. Miao, R. Ma and C. Wang, *Sol. Energy*, 2020, **203**, 25-31.
100. H. Wang, Z. Huang, S. Xiao, X. Meng, Z. Xing, L. Rao, C. Gong, R. Wu, T. Hu, L. Tan, X. Hu, S. Zhang and Y. Chen, *J. Mater. Chem. A*, 2021, **9**, 5759-5768.
101. J. Yang, T. Wang, Y. Li, X. Pu, H. Chen, Y. Li, B. Yang, Y. Zhang, J. Zhao, Q. Cao, X. Chen, S. Ghasemi, A. Hagfeldt and X. Li, *Sol. RRL*, 2022, **6**, 2200422.
102. Y. Hu, Z. Yang, X. Cui, P. Zeng, F. Li, X. Liu, G. Feng and M. Liu, *ACS Appl. Mater. Interfaces*, 2022, **14**, 13431-13439.
103. R. Islam, G. Chen, P. Ramesh, J. Suh, N. Fuchigami, D. Lee, K. A. Littau, K. Weiner, R. T. Collins and K. C. Saraswat, *ACS Appl. Mater. Interfaces*, 2017, **9**, 17201-17207.
104. Q. Lian, P.-l. Wang, G. Wang, X. Zhang, Y. Huang, D. Li, G. Mi, R. Shi, A. Amini, L. Zhang and C. Cheng, *Adv. Sci.*, 2022, **9**, 2201543.
105. J. F. Butscher, S. Intorp, J. Kress, Q. An, Y. J. Hofstetter, N. Hippchen, F. Paulus, U. H. F. Bunz, N. Tessler and Y. Vaynzof, *ACS Appl. Mater. Interfaces*, 2020, **12**, 3572-3579.
106. D. S. Mann, S.-N. Kwon, P. Patil and S.-I. Na, *Nano Energy*, 2023, **106**, 108062.
107. J. Zhang, J. Yang, R. Dai, W. Sheng, Y. Su, Y. Zhong, X. Li, L. Tan and Y. Chen, *Adv. Energy Mater.*, 2022, **12**, 2103674.
108. H. C. Weerasinghe, Y. Dkhissi, A. D. Scully, R. A. Caruso and Y.-B. Cheng, *Nano Energy*, 2015, **18**, 118-125.
109. Q. Emery, M. Remec, G. Paramasivam, S. Janke, J. Dagar, C. Ulbrich, R. Schlatmann, B. Stannowski, E. Unger and M. Khenkin, *ACS Appl. Mater. Interfaces*, 2022, **14**, 5159-5167.
110. A. Uddin, M. B. Upama, H. Yi and L. Duan, *Coatings*, 2019, **9**, 65.
111. G. S. Han, Y. H. Song, Y. U. Jin, J.-W. Lee, N.-G. Park, B. K. Kang, J.-K. Lee, I. S. Cho, D. H. Yoon and H. S. Jung, *ACS Appl. Mater. Interfaces*, 2015, **7**, 23521-23526.
112. G. S. Han, J. S. Yoo, F. Yu, M. L. Duff, B. K. Kang and J.-K. Lee, *J. Mater. Chem. A*, 2017, **5**, 14733-14740.
113. J. H. Jang, B.-J. Kim, J.-h. Kim, E. Han, E. Y. Choi, C. H. Ji, K.-T. Kim, J. Kim and N. Park, *ACS omega*, 2019, **4**, 9211-9218.
114. N. Rajamanickam, S. Kumari, V. K. Vendra, B. W. Lavery, J. Spurgeon, T. Druffel and M. K. Sunkara, *Nanotechnology*, 2016, **27**, 235404.